

X-Ray, DSC, TGA-dTGA, and Vibrational Studies of the Propylenediammonium Hexafluorosilicate $\text{NH}_3(\text{CH}_2)_3\text{NH}_3\text{SiF}_6$

Ali Ouasri^{1,2,*} , Ali Rhandour¹, Mohammed Saadi³ , Lahcen El Ammari³ 

¹ Laboratoire de Physico-Chimie des Matériaux Inorganiques, Faculty of Sciences, Ibn Tofaïl University, BO 133, 14000 Kenitra, Morocco

² Laboratoire (ReSIP), Centre Régional des Métiers de l'Éducation et de la Formation, Madinat Al Irfane, Souissi, BP 6210 Rabat, Morocco

³ Laboratoire de Chimie Appliquée des Matériaux, Centre des Sciences des Matériaux, Faculty of Sciences, Mohammed V University in Rabat, Avenue Ibn Batouta, B.P. 1014, Rabat, Morocco

* Correspondence: aouasri@yahoo.fr;

Scopus Author ID 56001570100

Received: 15.12.2020; Revised: 20.01.2021; Accepted: 23.01.2021; Published: 31.01.2021

Abstract: X-ray characterization, thermal behavior, and vibrational studies have been performed on $\text{NH}_3(\text{CH}_2)_3\text{NH}_3\text{SiF}_6$, which crystallized in the $P2_1/c$ ($Z = 4$) monoclinic system. The V/Z ratio variation (unit cell volume/ motifs number per cell) versus the CH_2 groups' number is discussed for $\text{H}_3\text{N}(\text{CH}_2)_n\text{NH}_3\text{SiF}_6$ salts ($n = 2, 3, 4, 6$). The DSC measurements (heating/cooling) recorded in the 35-245°C temperature domain showed the $\text{NH}_3(\text{CH}_2)_3\text{NH}_3\text{SiF}_6$ decomposition above 30 °C, which is checked and analyzed by TGA-dTGA techniques. The vibrational spectra interpretation is developed based on theoretical group analyses considering the $^+\text{NH}_3(\text{CH}_2)_3\text{NH}_3^+$ cations and the SiF_6^{2-} anions in the $C_1(4)$ and $C_i(2)$ symmetry sites, respectively. The SiF_6^{2-} degenerated modes splitting is explained by the site effect, resulting in symmetry lowering from O_h to C_i in the crystal. The Infrared spectrum analysis at lower N-H and C-H frequencies region showed the presence of medium to strong N-H...F hydrogen bonding in the title compound.

Keywords: propylenediammonium; hexafluorosilicate; X-ray; DSC; TGA-dTGA; IR; Raman; decomposition; site group; factor group.

© 2021 by the authors. This article is an open-access article distributed under the terms and conditions of the Creative Commons Attribution (CC BY) license (<https://creativecommons.org/licenses/by/4.0/>).

1. Introduction

Hexafluorosilicate compounds of the general formula $[\text{R}_{4-n}\text{NH}_n]_2\text{SiF}_6$ (R: alkyl, $n = 0, 1, 2, 3$) studied over the two last decades [1-16] have been found to present interesting crystal dynamic and phase transitions involving as well as hydrogen bonds and reorientation motions of alkylammoniums cations [1-8]. The temperature-dependent phase transitions in such compounds have been studied using differential scanning calorimetry (DSC), Raman spectroscopy at different temperatures, and optical properties.

The crystal structures, the physicochemical properties, and the anticaries activities of novel potential anticaries hexafluorosilicate substances are developed [14-22]. The pyridinium hexafluorosilicate salts $(\text{LH})_2\text{SiF}_6$ (L = 2-, 3-, 4-carboxymethylpyridine) with the general formula $(\text{C}_{14}\text{H}_{16}\text{N}_2\text{O}_4)_2\text{SiF}_6$ crystallized in the $(P2_1/n, Z = 2)$, $(P2_1/c, Z = 2)$, and $(I2/a, Z = 4)$, respectively [15]. Gelmboldt *et al.* [16] have developed a review study, summarizing the research results published mainly after 2000 on the synthetic protocols, structure, spectral

characteristics, solubility and hydrolysis, properties, and the practical application aspects of the hexafluorosilicate salts. This study reflected various aspects of the state of chemistry and applied use of hexafluorosilicate salts obtained up 2019: modifiers of zeolite catalysts, fluoridating agents, activating additives and catalysts, preparation of amorphous silica, ionic liquids, and electro-optical materials.

The biological activity analysis showed a low probability of toxic effects of the novel hexafluorosilicate $(\text{LH})_2\text{SiF}_6 \cdot \text{H}_2\text{O}$ (L: 3-hydroxymethylpyridine) compound [17]. Hexafluorosilicate salts with the substituted pyridinium and pyrimidinium cations exhibit antibacterial, anti-inflammatory, and other activity types, which leads to an experimentally confirmed increase in cariesprophylactic efficacy (CPE) of such substances compared to reference drugs [18]. It has been demonstrated that ammonium hexafluorosilicates, including salts with substituted biologically active ammonium cations, have a high cariesprophylactic efficacy [20, 21].

The hexafluorosilicate $\text{NH}_3(\text{CH}_2)_n\text{NH}_3\text{SiF}_6$ compounds, belonging to the alkylenediammonium hexahaloanometallate salts family $\text{NH}_3(\text{CH}_2)_n\text{NH}_3\text{MX}_6$ (M: Sn, Si; X: Cl, F) [23-31], are recently found to present interesting properties in catalysis [13-16, 23-30]. Research including X-ray diffraction, thermal, vibrational, and phase transitions studies have also been reported on alkylenediammonium chlorobismuthate salts $[\text{NH}_3(\text{CH}_2)_{12}\text{NH}_3]_2\text{BiCl}_6 \cdot \text{Cl} \cdot 2\text{H}_2\text{O}$ [32] and $\text{NH}_3(\text{CH}_2)_n\text{NH}_3\text{BiCl}_5$ [33-40].

The $\text{NH}_3(\text{CH}_2)_2\text{NH}_3\text{SiF}_6$, monoclinic of space group $P2_1/n$ ($Z = 2$), is the first compound studied among the alkylenediammonium hexafluorosilicate salts [25]. Its structure consisted of SiF_6^{2-} octahedra located on the inversion centres of the Wyckoff positions [2d (1/2, 1/2, 0); 2c (0, 0, 1/2)], and ethylenediammonium cations also placed on inversion centers [2a (0, 0, 0); 2b (1/2, 1/2, 1/2)]. The $^+\text{NH}_3(\text{CH}_2)_2\text{NH}_3^+$ cations and SiF_6^{2-} anions are linked with N-H...F hydrogen bonding, ensuring the three-dimensional cohesion of the crystal.

More recently, works reporting crystal structures, vibrational studies, DFT modeling, and catalysis have been made on two alkylenediammonium hexafluorosilicate compounds $\text{NH}_3(\text{CH}_2)_n\text{NH}_3\text{SiF}_6$ ($n = 4, 6$) [26-30]. The crystal structure of $\text{NH}_3(\text{CH}_2)_4\text{NH}_3\text{SiF}_6 P-1$ ($Z = 1$) consisted of the SiF_6^{2-} anion observed on an inversion center $C_i(1)$ compatible to the Wyckoff the position 1d (1/2, 0, 0), the bond C2-C2i center of the cation is placed on another inversion center [26]. The structure of $\text{NH}_3(\text{CH}_2)_6\text{NH}_3\text{SiF}_6 P-1$ ($Z = 2$), is built up from two SiF_6^{2-} anions and two organic cations $^+\text{NH}_3(\text{CH}_2)_6\text{NH}_3^+$ [25]. An anion Si1 is observed in the general position (x, y, z) of C_1 symmetry. The two moieties of anions are located at inversion centers: Si2 on the Wyckoff position 1g (0, 1/2, 1/2) and Si3 on 1a (0, 0, 0). The unit cell contains one organic cation and two halves of cations located at inversion centers.

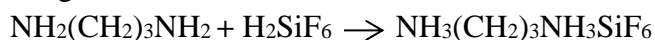
The hexafluorosilicate $\text{NH}_3(\text{CH}_2)_n\text{NH}_3\text{SiF}_6$ structure is monoclinic of space group $P2_1/n$ for ($n = 2$), triclinic of space group $P-1$ ($Z = 1$) when $n = 4$, and $P-1$ ($Z = 2$) for $n = 6$. In the $P2_1/n$ space group, there are 4 sets of non-equivalent inversion centers $4C_i(2)$, while in the $P-1$ there are 8 non-equivalent inversion centers $8C_i(1)$. In the $\text{NH}_3(\text{CH}_2)_n\text{NH}_3\text{SiF}_6$ structures, the $^+\text{NH}_3(\text{CH}_2)_n\text{NH}_3^+$ cations were linked to SiF_6^{2-} anions with N-H...F hydrogen bonds, ensuring the three-dimensional cohesion of the crystals.

In this work, we present X-ray, DSC, TGA-dTGA, Infrared, and Raman spectra studies carried out on $\text{NH}_3(\text{CH}_2)_3\text{NH}_3\text{SiF}_6$. The vibrational spectroscopy aiming to support the compound structural characterization by extracting the structure-spectra correlations is a powerful tool to describe the cations' behavior and their contribution to the distortion of the

SiF₆²⁻ octahedral structure. The free ions symmetry changed in the crystal structure, which influences the infrared and Raman bands' vibrational selection rules and assignment.

2. Materials and Methods

NH₃(CH₂)₃NH₃SiF₆ crystals were obtained by slow evaporation at room temperature of an aqueous solution containing stoichiometric amounts of alkylenediamine NH₂(CH₂)₃NH₂ and H₂SiF₆ acid, following the chemical reaction, described as:



A single crystal is carefully selected using a polarizing microscope. Data are collected at room temperature using the Bruker Apex2 AXS X8 diffractometer equipped with a CCD detector and a graphite monochromator for Mo K α radiation ($k = 0.71073 \text{ \AA}$).

The powder of NH₃(CH₂)₃NH₃SiF₆ compound is characterized at room temperature by the X-ray diffraction method using an XRD-XPRT PRO-Panalytical performed with Bragg-Brentano geometry and CuK α radiation. ($\lambda = 1.5418 \text{ \AA}$). The XRD pattern is performed in the range of 2θ between 10° and 90° with 40 kV and 50 mA operating conditions.

The differential scanning calorimetric measurements were performed on the powdered compound in a DSC-Q100 calorimeter (from TA Instruments) using sample masses 6.39 mg in a hermetic aluminum sample holder, from 45°C to 245°C at a heating and cooling rate of 5°C min^{-1} under nitrogen atmosphere, flowing at 50 mL min^{-1} .

The thermogravimetric analyses (TGA-dTGA) of the compound have been performed with a TA Instruments balance model STA-1640. It allows for obtaining simultaneous TGA and dTGA diagrams under similar experimental conditions. Experiments were performed under a nitrogen atmosphere, from 30°C to 245°C at a heating rate of 5°C/min . About 12.683 mg of the compound was used initially for these measurements.

The Infrared spectrum was recorded in the $450\text{-}4000 \text{ cm}^{-1}$ spectral range with a 4 cm^{-1} resolution (64 scans), by using a VERTEX 70 FTIR spectrometer (produced by BRUKER Optics). The crystals were ground in a clean mortar to a fine powder. The MIR Transmission Technic was used to record the IR spectrum.

The Raman spectra were recorded at room temperatures, in the $25\text{-}3500 \text{ cm}^{-1}$ by using a RAM spectrometer (220 mw) coupled with the VERTEX 70, and equipped with the exciting source Laser of a radiation wavelength (455 nm) and a puissance laser of 6.0 mw.

3. Results and Discussion

3.1. X-ray characterization.

The single crystal X-Ray diffraction characterization carried out on NH₃(CH₂)₃NH₃SiF₆ at ambient temperature showed that the title compound crystallizes in the monoclinic system with $P2_1/c$ ($Z = 4$) as space group [$a = 18.871(4) \text{ \AA}$, $b = 5.879(2) \text{ \AA}$, $c = 17.345(3) \text{ \AA}$; $\beta = 117.331(3)$, $V = 1709.44 \text{ \AA}^3$]. The full crystal structure is not yet determined with a satisfactory, reliable coefficient R. The ambient temperature powder X-ray diffractogram shown in Figure 1 indicates that the title compound is well crystallized.

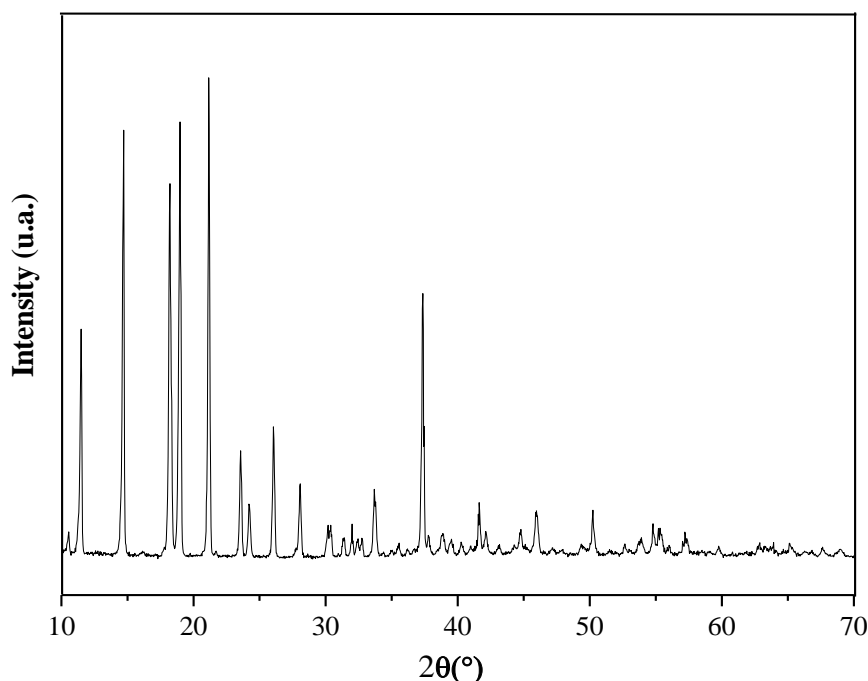


Figure 1. The powder X-Ray diffractogram of $\text{NH}_3(\text{CH}_2)_3\text{NH}_3\text{SiF}_6$ compound measured at ambient temperature.

The single-crystal structures of $\text{NH}_3(\text{CH}_2)_n\text{NH}_3\text{SiF}_6$ ($n = 2, 4, 6$) salts have been completely determined [25-27], which allowed us to make a comparative study between these compounds' structures. Based on the crystallographic data obtained for these compounds (Table 1), one can predict the structure of $\text{NH}_3(\text{CH}_2)_3\text{NH}_3\text{SiF}_6$, which is not fully determined until now. The $\text{NH}_3(\text{CH}_2)_n\text{NH}_3\text{SiF}_6$ ($n = 2, 3$) compounds crystallized in the monoclinic system with the space groups ($P2_1/n$, $Z = 2$) for $n = 2$ and ($P2_1/c$, $Z = 4$) for $n = 3$, with different lattice parameters and unit cell volume values (Table 1). The changes concern particularly the (Z , β , V) parameters when passing from (2; $93.84(1)^\circ$; $148.13(7) \text{ \AA}^3$) in the compound with ($n = 2$) to (4; 117° ; 1702 \AA^3) in the present studied compound ($n = 3$).

Table 1: Crystallographic data of the alkylenediammonium hexafluorosilicate compounds

Compounds	System	Space group	Unit cell parameters	References
$\text{NH}_3(\text{CH}_2)_2\text{NH}_3\text{SiF}_6$	Monoclinic	$P2_1/n$ ($Z = 2$)	$a = 7.351(3) \text{ \AA}$ $b = 8.732(3) \text{ \AA}$ $c = 5.819(2) \text{ \AA}$ $\beta = 93.84(1)^\circ$ $V = 148.13(7) \text{ \AA}^3$	[23]
$\text{NH}_3(\text{CH}_2)_3\text{NH}_3\text{SiF}_6$	Monoclinic	$P2_1/c$ ($Z = 4$)	$a = 17.34 \text{ \AA}$ $b = 5.88 \text{ \AA}$ $c = 18.86 \text{ \AA}$ $\beta = 117^\circ$ $V = 1702 \text{ \AA}^3$	Present work
$\text{NH}_3(\text{CH}_2)_4\text{NH}_3\text{SiF}_6$	Triclinic	$P-1$ ($Z = 1$)	$a = 5.796(1) \text{ \AA}$ $b = 5.889(1) \text{ \AA}$ $c = 7.774(2) \text{ \AA}$ $\alpha = 87.02(1)^\circ$ $\beta = 82.15(1)^\circ$ $\gamma = 61.87(1)^\circ$ $V = 231.79(8) \text{ \AA}^3$	[24]
$\text{NH}_3(\text{CH}_2)_6\text{NH}_3\text{SiF}_6$	Triclinic	$P-1$ ($Z = 2$)	$a = 5.8965(2) \text{ \AA}$ $b = 13.6946(5) \text{ \AA}$ $c = 14.4945(5) \text{ \AA}$ $\alpha = 91.379(2)^\circ$ $\beta = 92.797(2)^\circ$ $\gamma = 90.906(2)^\circ$ $V = 1168.53(7) \text{ \AA}^3$	[25]

The structure of $\text{NH}_3(\text{CH}_2)_3\text{NH}_3\text{SiF}_6$ compound may be built up from four SiF_6^{2-} anions located on the moiety of the inversion centers $4C_i(2)$ corresponding to the Wyckoff positions of the space group [2a, 2b, 2c, 2d] and four propylenediammonium cations placed on the general positions $C_1(4)$ compatible with the Wyckoff positions 4e. The non-centrosymmetric $^+\text{NH}_3(\text{CH}_2)_3\text{NH}_3^+$ cations are assumed to be of C_1 symmetry. The anions may be linked to the organic cations through hydrogen bonds, which are characteristic of organic-inorganic hexafluorosilicate compounds [25-27].

The V/Z ratio variation (V: cell volume, Z: number of motifs per cell) versus the CH_2 groups' number (n = 2, 3, 4, 6) in the $\text{NH}_3(\text{CH}_2)_n\text{NH}_3\text{SiF}_6$ compounds is given in Figure 2. The variation is not linear. A deviation is observed when going from n = 3 to 4, i.e., when passing from the monoclinic system observed for the compounds (n = 2, 3) to the compounds' triclinic system (n = 4, 6). The change from the monoclinic symmetry to the triclinic one occurs with an appreciable deviation in the unit cell volume values.

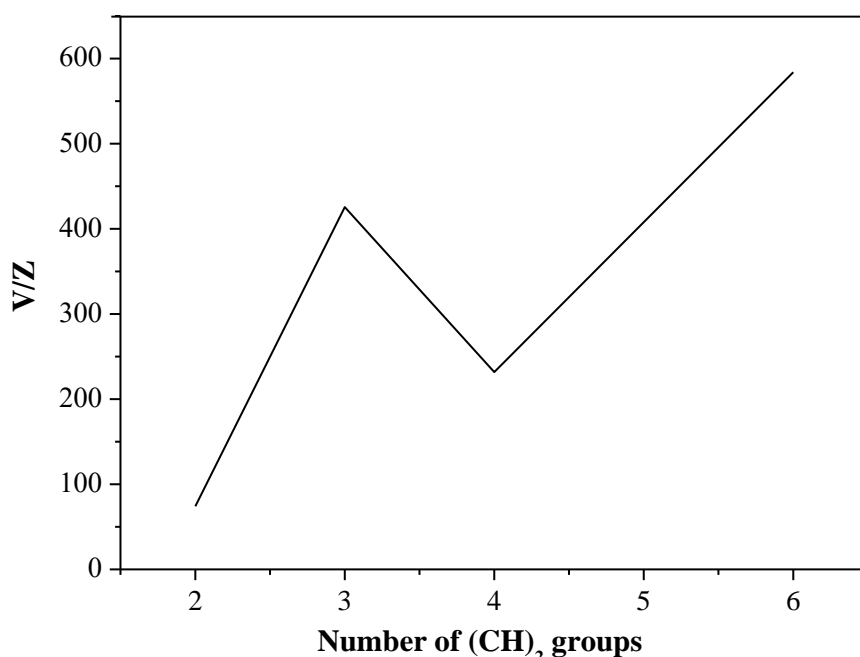


Figure 2. The variation of the cell volume (V) / number of motif per cell (Z) with number “n” of (CH₂) groups in the hexafluorosilicate $\text{NH}_3(\text{CH}_2)_n\text{NH}_3\text{SiF}_6$ (n = 2, 3, 4, 6).

3.2. Thermal behavior analyses.

3.2.1. Differential scanning calorimetry (DSC).

The DSC curves of $\text{NH}_3(\text{CH}_2)_3\text{NH}_3\text{SiF}_6$ recorded between 35 and 245°C are shown in Figure 3. In heating, a strong and broad peak was centered around 125°C, which is not observed in the cooling. The irreversible heating anomaly indicates the title compound's decomposition process, which takes place above 30°C. To check that the compound is not stable, we have carried out the TG-dTG analyses in the studied DSC temperature domain.

3.2.2. Thermogravimetric (TG-dTG).

The thermogravimetric (TGA- dTG) curves of $\text{NH}_3(\text{CH}_2)_3\text{NH}_3\text{SiF}_6$ were recorded on heating runs (5 °C.min⁻¹) between 30°C and 245°C (Figure 4). The initial weight of the crystal used in the TG-dTG analyses is $m_i = 10.291$ mg. The thermal decomposition process of the title compound begins at 30°C. As shown in Figure 4, the compound's weight loss is 57.8 %

over the decomposition process (30-245°C). The compound decomposition is illustrated by the endothermic DSC anomaly, which appeared at around 125°C.

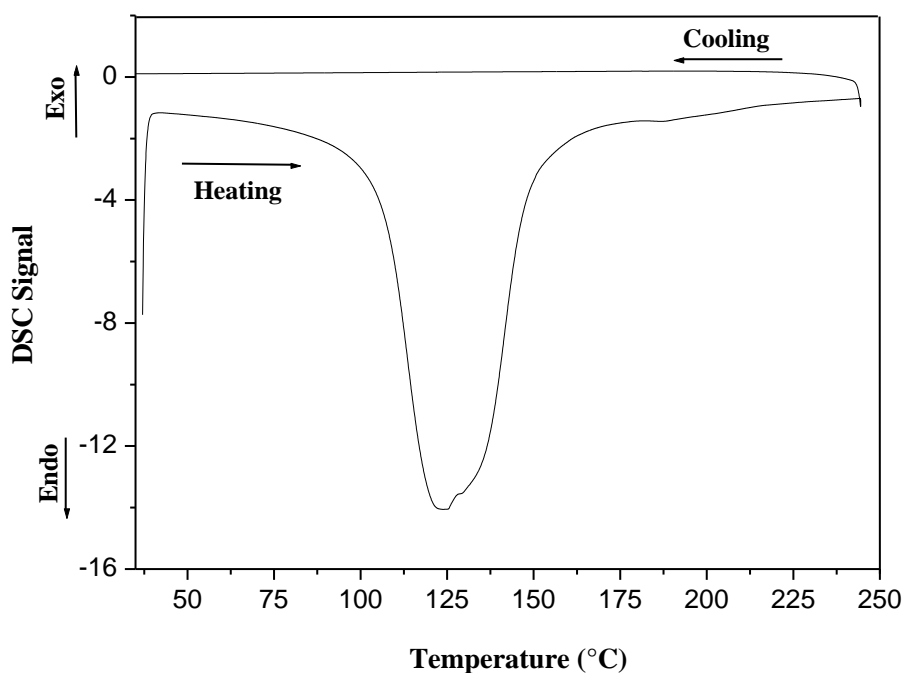


Figure 3. DSC curves of $\text{NH}_3(\text{CH}_2)_n\text{NH}_3\text{SiF}_6$ compound on heating and cooling runs ($10^\circ\text{C min}^{-1}$) in the 35-245 °C temperature range.

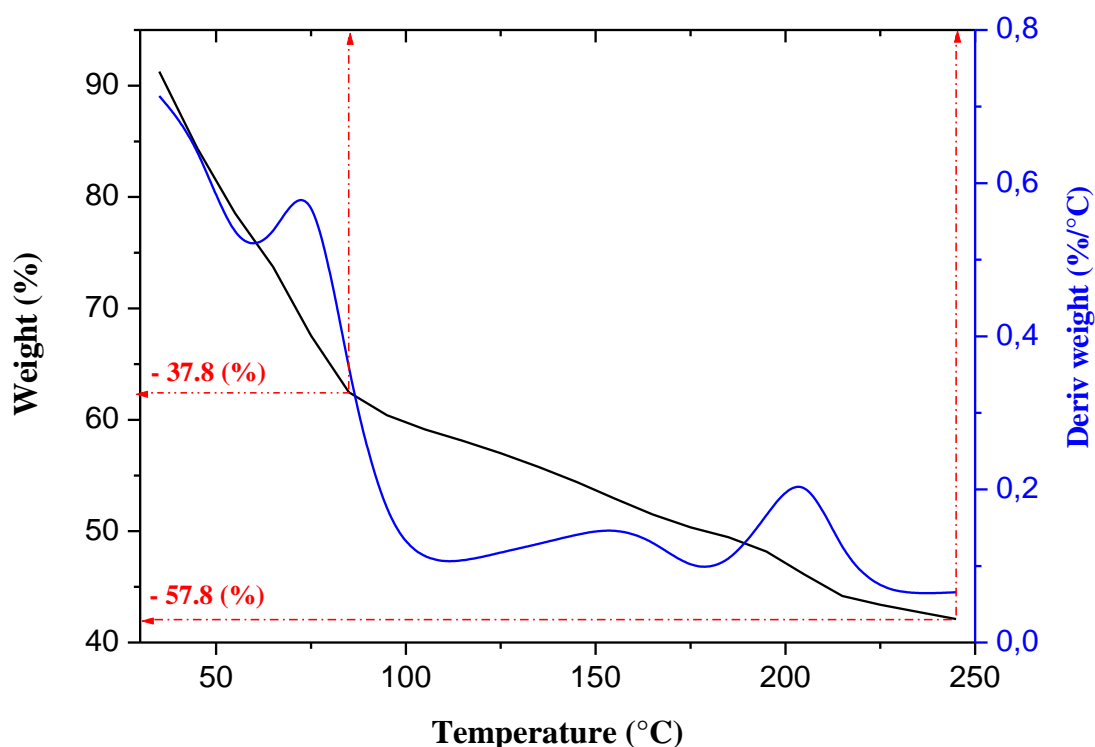
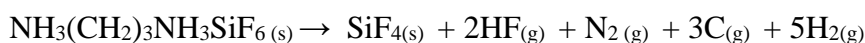


Figure 4. TG-dTG curves (5°C.min^{-1}) measured for $\text{NH}_3(\text{CH}_2)_n\text{NH}_3\text{SiF}_6$ in the 35-245°C temperature range.

The estimated weight loss at 85°C [$\Delta m/m_i = 37.8\%$, i.e. $\Delta m = 3.89\text{ mg}$] is due to the first decomposition step of the crystal. The second decomposition step is made between 85 °C and 245°C, giving rise to the estimated total weight loss : $\Delta m/m_i = 57.8\%$ (i.e. $\Delta m = 5.95\text{ mg}$). Based on literature data [41-43], the $\text{NH}_3(\text{CH}_2)_3\text{NH}_3\text{SiF}_6$ thermal decomposition may be described by the proposed equation:



The equation suggests that each mole of $\text{NH}_3(\text{CH}_2)_3\text{NH}_3\text{SiF}_6$ ($218.1 \text{ g}\cdot\text{mol}^{-1}$) gives 3 moles of carbon ($36 \text{ g}\cdot\text{mol}^{-1}$), 5 moles of H_2 ($4 \text{ g}\cdot\text{mol}^{-1}$), 1 mole of N_2 , 2 moles of HF ($20 \text{ g}\cdot\text{mol}^{-1}$), and 1 mole of SiF_4 ($104.1 \text{ g}\cdot\text{mol}^{-1}$). The calculated $m(\text{C})$, $m(\text{H}_2)$, $m(\text{N}_2)$, and $m(\text{HF})$ in the initial crystal weight are given as the following:

$$[m(\text{C}) = (m_i/218.1) \times 3M(\text{C}) = (10.291/218.1) \times 36 = 1.6987 \text{ mg}]$$

$$[m(\text{H}_2) = (m_i/218.1) \times 10M(\text{H}) = (10.291/218.1) \times 10 = 0.4718 \text{ mg}]$$

$$[m(\text{N}_2) = (m_i/218.1) \times 2M(\text{N}) = (10.291/218.1) \times 28 = 1.3212 \text{ mg}]$$

$$[m(\text{HF}) = (m_i/218.1) \times 2M(\text{HF}) = (10.291/218.1) \times 40 = 1.8874 \text{ mg}]$$

As indicated in Figure 4, the first decomposition step is done at 37.8% with an estimate weight loss of $\Delta m = 3.89 \text{ mg}$, which is nearly close to the calculated mass for the C, H_2 , and N_2 in the initial crystal weight [$m(\text{C}) + m(\text{H}_2) + m(\text{N}_2) = 3.4917 \text{ mg}$]. Over the second decomposition step, the estimated total weight loss at 245°C is $\Delta m = 5.95 \text{ mg}$ (Figure 4). This value is close to the loss weight calculated as [$m(\text{C}) + m(\text{H}_2) + m(\text{N}_2) + m(\text{HF}) = 5.3791 \text{ mg}$]. At this temperature, the remaining $m(\text{SiF}_4)$ in the initial crystal weight is calculated as: [$(10.291/218.1) \times 104.1 = 4.9119 \text{ mg}$].

The TGA-dTG analyses indicate the title compound's decomposition processes over the $30\text{-}245^\circ\text{C}$ temperature domain, as highlighted by the DSC technique in the corresponding temperature domain.

3.3. Group theoretical analyses.

The theoretical group analysis of the number and the symmetry of the normal modes is developed according to the crystal structure data obtained from the XRD study of $\text{NH}_3(\text{CH}_2)_3\text{NH}_3\text{SiF}_6$ compound, which is a monoclinic system, $P2_1/c$ ($Z = 4$) space group.

3.3.1. Vibrational modes of $^+\text{NH}_3(\text{CH}_2)_3\text{NH}_3^+$ cation.

The free $^+\text{NH}_3(\text{CH}_2)_3\text{NH}_3^+$ cation considered in the C_{2v} symmetry displays 45 internal vibrational modes described as $14 \text{ A}_1(\text{Ra, IR}) + 9 \text{ A}_2(\text{Ra}) + 10 \text{ B}_1(\text{Ra, IR}) + 10 \text{ B}_2(\text{Ra, IR})$. Within the crystal of space group $P2_1/c$ ($Z = 4$) (C_{2h}^5), the $^+\text{NH}_3(\text{CH}_2)_3\text{NH}_3^+$ cations are assumed to occupy the general positions of Wyckoff positions (4e) and are considered C_1 symmetry sites.

Table 2. Correlation diagram of $^+\text{NH}_3(\text{CH}_2)_3\text{NH}_3^+$ internal vibrational modes in the crystal.

Molecular group (C_{2v})	Site group (C_1)	Factor group (C_{2h})
14 $\text{A}_1(\text{Ra, IR})$	45 A (Ra, IR)	45 $\text{A}_g(\text{Ra})$
9 $\text{A}_2(\text{Ra})$		45 $\text{A}_u(\text{IR})$
10 $\text{B}_1(\text{Ra, IR})$		45 $\text{B}_g(\text{Ra})$
12 $\text{B}_2(\text{Ra, IR})$		45 $\text{B}_u(\text{IR})$

In the C_1 site group (Table 2), the cationic vibrational modes are of the A symmetry, all infrared, and Raman active. By the crystal field effect (Davydov splitting effect) due to the existence of 4 cations per primitive unit cell, each of 45 A internal modes of cations in the site group should theoretically split into four components (A_g , B_g) active in Raman and (A_u , B_u)

actives in Infrared. So, the 180 cationic internal modes predicted in the crystal are described as [45 A_g (Ra) + 45 A_u (IR) + 45 B_g (Ra) + 45 B_u (IR)]; the *gerade* modes are Raman actives, whereas the *ungerade* are infrared actives in respect of the selection rules implied by the centrosymmetric of the crystal.

3.3.2. Vibrational modes of SiF_6^{2-} anion.

The free SiF_6^{2-} anion of O_h symmetry undergoes 15 internal normal modes, which are classified as: $1A_{1g}$ (R) + $1E_g$ (R) + $1F_{2g}$ (R) + $2F_{1u}$ (IR) + $1F_{2u}$ (In). The vibrational modes (A_{1g} , E_g , F_{2g}) are Raman-active; those of F_{1u} type are infrared active and should appear as single bands, whereas the F_{2u} modes are inactive.

In the crystal of the $P2_1/c$ ($Z = 4$) space group, the SiF_6^{2-} anions are assumed to occupy the sites' symmetry C_i (2). By the site effect (Table 3), the A_{1g} , E_g , F_{2g} modes become of A_g symmetry, with splitting of E_g and F_{2g} modes into two and three Raman active components, respectively. Besides, the infrared active F_{1u} and the inactive F_{2u} modes become split each other into three components of A_u symmetry, all active in Infrared. Under the crystal field effect (Davydov splitting effect), the *gerade* modes A_g should split into two (A_g , B_g) active in Raman, and the *ungerade* F_{1u} to two components (A_u , B_u) active in Infrared. This gives in the group factor 180 internal modes described as [45 A_g (Ra) + 45 A_u (IR) + 45 B_g (Ra) + 45 B_u (IR)]. Splitting of the vibrational modes in the solid-state is expected for SiF_6^{2-} in the crystal by lowering of the symmetry ($O_h \rightarrow C_i$).

Table 3. Correlation diagram of SiF_6^{2-} internal vibrational modes in the crystal.

Molecular symmetry (O_h)	Site symmetry (C_i)	Factor Group (C_{2h})
$v_1: 1 A_{1g}$ (Ra)	A_g (Ra)	45 A_g (Ra)
$v_2: 1 E_g$ (Ra)		
$v_5: 1 F_{2g}$ (Ra)	A_u (IR)	45 A_u (IR)
$v_3, v_4: 2 F_{1u}$ (IR)		
$v_6: 1 F_{2u}$ (In)		
		45 B_g (Ra)
		45 B_u (IR)

3.4. Infrared and Raman spectra interpretation.

The Raman spectrum of $\text{NH}_3(\text{CH}_2)_3\text{NH}_3\text{SiF}_6$ is presented in Figure 5. The Infrared spectrum is divided into two regions ($4000\text{-}1800\text{ cm}^{-1}$, $1800\text{-}400\text{ cm}^{-1}$) as illustrated in Figures 6 (a-b). The vibrational spectra study is assisted by the normal vibrational modes predicted by the theoretical group analysis (Tables 2 and 3) and previous work on alkylammonium and alkylendiammonium salts [23, 28, 44-46]. The IR spectrum of the title compound is similar to those of $\text{NH}_3(\text{CH}_2)_n\text{NH}_3\text{SiF}_6$ ($n = 4, 6$) [28], which confirms the existence of the SiF_6^{2-} and the cations $^+\text{NH}_3(\text{CH}_2)_3\text{NH}_3^+$ in the present compound.

The Raman spectrum (Figure 5) highlights little clear bands observed at 2995, 960, 654 cm^{-1} , which can be assigned to the $\nu_{\text{as}}(\text{CH}_2)$, $\nu_{\text{as}}(\text{CN})$, and ν_1 (ν_s Si-F) vibrational modes. These peaks refer to the organic and inorganic components. It is observed the fluorescent shape which ascribes to the organic and inorganic parts in the Raman spectrum, which infers that the structural characterization of the bulk crystal is not efficient. It is to note that the more resolved

spectrum for the studied crystal is observed at the fixed power $P = 6.0$ mW, with the wavelength Laser at 455 nm.

The infrared spectrum of $\text{NH}_3(\text{CH}_2)_3\text{NH}_3\text{SiF}_6$ in the $3300\text{-}2800\text{ cm}^{-1}$ region contains appreciable bands due to N-H and C-H stretching modes of NH_3 and $(\text{CH}_2)_3$ groups (Figure 6.a). The weak IR band observed at 3207 cm^{-1} , and the strong band at 3063 cm^{-1} are assigned to asymmetric $\nu_{\text{as}}(\text{NH}_3)$ and symmetric $\nu_{\text{s}}(\text{NH}_3)$ stretching modes, respectively. The two strong IR bands observed at 3009 and 2960 cm^{-1} with a shoulder at 2980 cm^{-1} correspond to the CH_2 asymmetric stretching modes $\nu_{\text{as}}(\text{CH}_2)$, which give rise to a strong band in the Raman spectrum at 2995 cm^{-1} . The medium IR band located at 2893 cm^{-1} corresponds to the CH_2 symmetric stretching modes $\nu_{\text{s}}(\text{CH}_2)$.

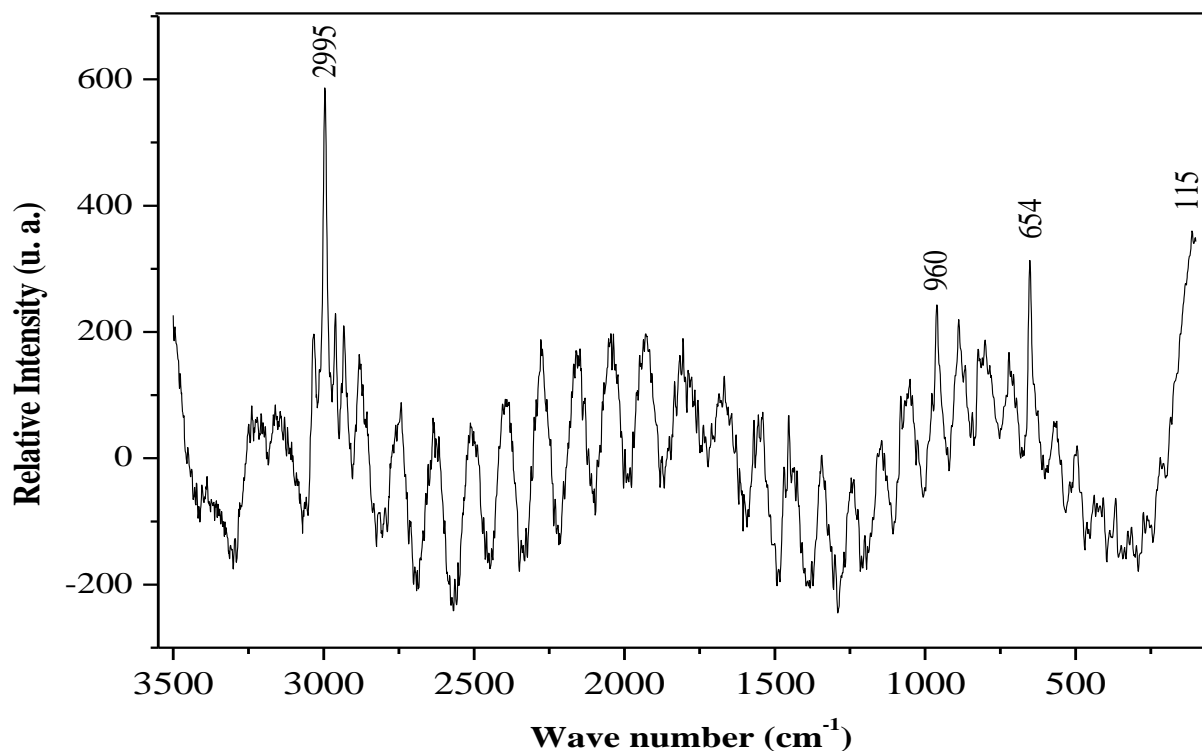


Figure 5. The Ramanspectrum of $\text{NH}_3(\text{CH}_2)_3\text{NH}_3\text{SiF}_6$ was recorded at ambient temperature in the $4000\text{-}25\text{ cm}^{-1}$ spectral range.

At lower wavenumbers of NH and CH stretching spectral region (Figure 6a), the non-fundamental bands of weak to medium intensities observed between 2768 and 1965 cm^{-1} are originated by the Fermi resonance between the fundamental CH_2 stretching and the overtone or combination bands of CH_2 bending modes, as has been found in several hybrid compounds [2, 4, 28]. The appearance of these modes with appreciable intensities at lower NH and CH stretching frequencies is an indication that hydrogen bonding N-H...F takes place between anions and cation in the $\text{NH}_3(\text{CH}_2)_3\text{NH}_3\text{SiF}_6$ compound. The assignment of the IR non-fundamental bands to combination and overtone modes is proposed in Table 5.

The medium bands observed at 1630 and 1600 cm^{-1} (Figure 6b) were attributed to the asymmetric bending modes $\delta_{\text{as}}(\text{NH}_3)$ (scissoring). The spectral range $1500\text{-}1190\text{ cm}^{-1}$ of the title compound consists of bands owing to the bending CH_2 modes of the $(\text{CH}_2)_3$ chains. As previously suggested, these bands are spread over a large spectral region [23, 28, 44]. Indeed, the strong IR bands observed at 1478 cm^{-1} and 1463 cm^{-1} were assigned to the $\delta(\text{CH}_2)$ scissoring modes (Table 4). The wagging and twisting CH_2 vibrational modes are observed in the 1410-

1215 cm^{-1} frequency region; the $\delta(\text{CH}_2)$ wagging modes exhibit a medium IR band at 1409 cm^{-1} , whereas the $\delta(\text{CH}_2)$ twisting modes give rise to a band of medium intensity at 1217 cm^{-1} .

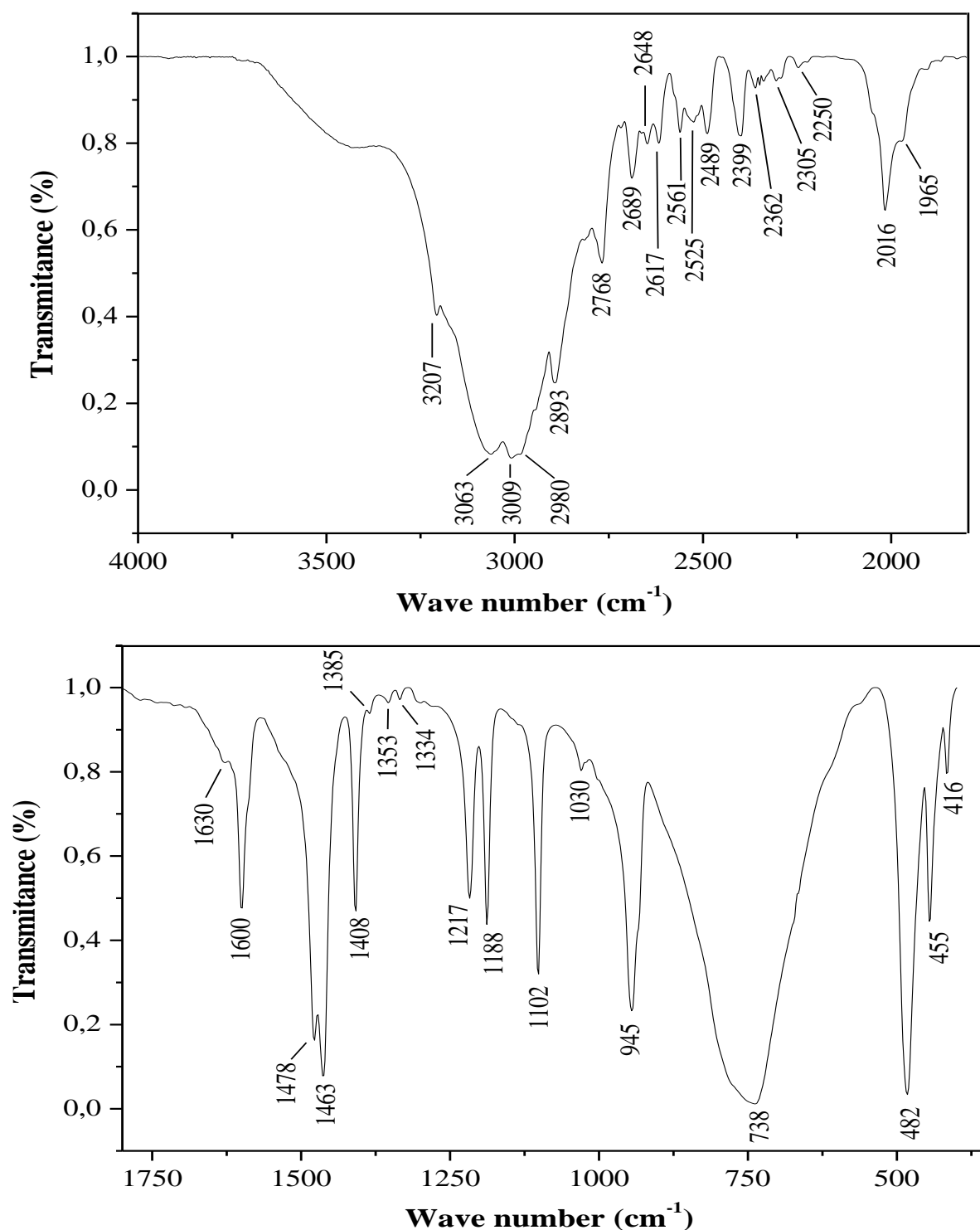


Figure 6. (a) The Infrared spectrum of $\text{NH}_3(\text{CH}_2)_3\text{NH}_3\text{SiF}_6$ recorded at room temperature in the 4000-1800 cm^{-1} spectral range; (b) The Infrared spectrum of $\text{NH}_3(\text{CH}_2)_3\text{NH}_3\text{SiF}_6$ recorded at ambient temperature in the 1800-400 cm^{-1} spectral range.

Other bands of weak intensities due to $\delta(\text{CH}_2)$ wagging and twisting are observed in this region (Table 4). The rocking CH_2 vibrations were found at lower frequencies as medium to strong bands in the 1220-730 cm^{-1} frequency range, as illustrated in Table 4. The vibrational modes involving C-C and C-N stretching modes were observed in the 1190-940 cm^{-1} spectral region. In the alkylene chain, they are generally mixed with the CH_2 and NH_3 wagging and

rooking modes [23, 28, 44]. The weak IR band observed at 1030 cm^{-1} is assigned to the $\nu(\text{C}-\text{C})$ stretching vibrations; the strong band located at 945 cm^{-1} may be due to the $\nu(\text{C}-\text{N})$ modes. The skeletal bending modes $\delta(\text{CCN})$ and $\delta(\text{CCC})$ may contribute to the strong and broadband observed at 445 cm^{-1} , while the $\delta_s(\text{CNC})$ are observed at 416 cm^{-1} as weak band.

The vibrational modes of the SiF_6^{2-} anions were generally observed below 700 cm^{-1} as shown in the Infrared spectrum (Figure 6.b) and Table 4. The theoretical analysis of the IR and Raman vibrational modes of the SiF_6^{2-} anion in O_h and C_i symmetries is shown in Table 3, suggesting normal modes are splitting by lowering the anion symmetry. This may reliably support the vibrational assignments made particularly in the Infrared spectrum. The results obtained are compared to the literature data [4, 11, 12].

In the Infrared spectrum, the four bands observed at 738, 482, 445, and 416 cm^{-1} may be due to the SiF_6^{2-} anions' vibrational modes. Indeed, the strong and broadband observed at 738 cm^{-1} may be originated from the $\nu_3(\nu_{\text{as}} \text{Si-F})$ modes of F_{1u} symmetry, which theoretically should be Infrared active (Table 3). The broadening of this band may have resulted as well in the splitting of the $\nu_3(\nu_{\text{as}} \text{Si-F})$ vibrational mode in the crystal (C_i factor group) and in the overlapping of other modes coming from the cationic skeletal such as $\delta(\text{CCN})$ and $\delta(\text{CCC})$ vibrations. The $\nu_4(\delta_{\text{as}} \text{F-Si-F})$ modes of symmetry F_{1u} are observed at 482 cm^{-1} as a very strong band. At 445 cm^{-1} as a medium band, confirming the splitting of these degenerated modes as predicted theoretically in Table 4.

In agreement with the C_i factor group analysis, the Raman active modes of symmetry A_g [$\nu_1(\nu_s \text{Si-F})$], E_g [$\nu_2(\nu_s \text{Si-F})$] and F_{2g} [$\nu_5(\delta_s \text{F-Si-F})$] are not activated in the infrared spectrum of the title compound, which well confirms the predicted C_i symmetry assigned to the anions in the crystal. The $\nu_1(\nu_s \text{Si-F})$ modes are observed only in the Raman spectrum as a medium band at 654 cm^{-1} ; the other modes $\nu_2(\nu_s \text{Si-F})$ and $\nu_5(\delta_s \text{F-Si-F})$ are not appreciably observed due to the fluorescence ascribing to the anionic and cationic parts of the $\text{NH}_3(\text{CH}_2)_3\text{NH}_3\text{SiF}_6$ Raman spectrum.

Table 4. Assignment of Infrared and some Raman bands of $\text{NH}_3(\text{CH}_2)_3\text{NH}_3\text{SiF}_6$.

IR	Raman	Assignment
3207 w		$\nu_{\text{as}}(\text{NH}_3)$
3063 s		$\nu_s(\text{NH}_3)$
3009 s	2995 s	$\nu_{\text{as}}(\text{CH}_2)$
2980 sh		
2960 s		
2893 m		
1630 m		$\delta_{\text{as}}(\text{NH}_3)$
1600 m		$\delta_{\text{as}}(\text{NH}_3)$
1478 s		$\delta(\text{CH}_2)_{\text{sci}} / \delta_s(\text{NH}_3)$
1463 vs		$\delta(\text{CH}_2)_{\text{sci}}$
1409 m		$\delta(\text{CH}_2)_{\text{wag}} + \nu(\text{CC})$
1385 vw		$\delta(\text{CH}_2)_{\text{wag}} + \nu(\text{CC})$
1353 w		$\delta(\text{CH}_2)_{\text{tw}}$
1334 w		$\delta(\text{CH}_2)_{\text{tw}}$
1217 m		$\delta(\text{CH}_2)_{\text{tw}} / \delta(\text{CH}_2)_{\text{rok}}$
1188 m		$\delta(\text{CH}_2)_{\text{rok}} + \nu(\text{CC})$
1102 s		$\delta(\text{NH}_3)_{\text{rok}}$
1030 w		$\nu(\text{CC})$
	960 m	$\nu_{\text{as}}(\text{CN})$
945 s		$\delta(\text{NH}_3)_{\text{rok}} + \nu(\text{CN})$
738 s, b		$\nu_3(\nu_{\text{as}} \text{Si-F}) / \delta(\text{CH}_2)_{\text{rok}}$
	654 m	$\nu_1(\nu_s \text{Si-F})$
482 vs		$\nu_4(\delta_{\text{as}} \text{F-Si-F})$
445 m		$\nu_4(\delta_{\text{as}} \text{F-Si-F}) / \delta(\text{CCN}) / \delta(\text{CCC})$

IR	Raman	Assignment
416 w		δ_s (CNC)
	115 m	Lattice modes

vs :very strong, s: strong, m: medium, vw: very weak, w: weak, b: broad, sh: shoulder

Table 5. Assignment of the non-fundamental Infrared bands of $\text{NH}_3(\text{CH}_2)_3\text{NH}_3\text{SiF}_6$ (m: medium, w: weak, vw: very weak).

Band (cm^{-1})	Assignment
2768 m	$\approx 2762 = 1409 + 1353 : [\delta(\text{CH}_2)_{\text{wag}}/\nu(\text{C-C}) + \delta(\text{CH}_2)_{\text{twi}}]$
2689 m	$\approx 2680 = 1463 + 1217 : [\delta(\text{CH}_2)_{\text{sci}} + \delta(\text{CH}_2)_{\text{twi}}/\delta(\text{CH}_2)_{\text{rok}}]$
2648 w	$\approx 2651 = 1463 + 1188 : [\delta(\text{CH}_2)_{\text{sci}} + (\text{CH}_2)_{\text{rok}}/\nu(\text{C-C})]$
2617 w	$\approx 2626 = 1409 + 1217 : [\delta(\text{CH}_2)_{\text{wag}}/\nu(\text{C-C}) + \delta(\text{CH}_2)_{\text{twi}}/\delta(\text{CH}_2)_{\text{rok}}]$
2561 w	$\approx 2565 = 1463 + 1102 : [\delta(\text{CH}_2)_{\text{sci}} + \delta(\text{NH}_3)_{\text{rok}}]$
2525 w	$\approx 2511 = 1409 + 1102 : [\delta(\text{CH}_2)_{\text{wag}}/\nu(\text{C-C}) + \delta(\text{NH}_3)_{\text{rok}}]$
2489 w	$\approx 2493 = 1463 + 1030 : [\delta(\text{CH}_2)_{\text{sci}} + \nu(\text{C-C})]$
2399 m	$\approx 2408 = 1463 + 945 : [\delta(\text{CH}_2)_{\text{sci}} + \delta(\text{NH}_3)_{\text{rok}}/\nu(\text{C-N})]$
2362 w	$\approx 2364 = 1334 + 1030 : [\delta(\text{CH}_2)_{\text{twi}} + \nu(\text{C-C})]$
2305 w	$\approx 2298 = 1353 + 945 : [\delta(\text{CH}_2)_{\text{twi}}/\delta(\text{NH}_3)_{\text{rok}}/\nu(\text{C-N})]$
2250 w	$\approx 2247 = 1217 + 1030 : [\delta(\text{CH}_2)_{\text{twi}}/\delta(\text{CH}_2)_{\text{rok}} + \nu(\text{C-C})]$
2016 m	$\approx 2016 = 1600 + 416 : [\delta_{\text{as}}(\text{NH}_3) + \delta_s(\text{C-N-C})]$
1965 w	$\approx 1975 = 1030 + 945 : [\nu(\text{C-C}) + \delta(\text{NH}_3)_{\text{rok}}/\nu(\text{C-N})]$

4. Conclusions

The single X-Ray characterization showed that the $\text{NH}_3(\text{CH}_2)_3\text{NH}_3\text{SiF}_6$ compound crystallized in the monoclinic system with the space group $\text{P2}_1/\text{c}$ ($Z = 4$). The V/Z ratio variation (cell volume/motifs number per cell) versus the CH_2 groups' number were compared and discussed for the $\text{NH}_3(\text{CH}_2)_n\text{NH}_3\text{SiF}_6$ compounds ($n = 2, 3, 4, 6$).

The DSC measurements recorded in heating and cooling ($35\text{-}245^\circ\text{C}$) showed that the unstable title compound undergoes a decomposition process above 30°C . This thermal behavior is well checked and verified by TGA-dTGA analyses.

The number and symmetry of the IR and Raman active modes of $\text{NH}_3(\text{CH}_2)_3\text{NH}_3\text{SiF}_6$ were determined by the factor group analysis to support the vibrational spectra interpretation. Splitting bands observed in the spectra are caused by the site effects on the degenerate internal modes of SiF_6^{2-} anions due to lower symmetry in the crystal structure from O_h to C_i . The $^+\text{NH}_3(\text{CH}_2)_3\text{NH}_3^+$ cations are considered in the $\text{C}_1(4)$ symmetry sites. The Infrared analysis highlights the presence of hydrogen bonding in this compound.

Funding

This research received no external funding.

Acknowledgments

This research has no acknowledgment.

Conflicts of Interest

The authors declare no conflict of interest.

References

1. Jeghnou, H.; Ouasri, A.; Elyoubi, M.; Rhandour, A.; Dhamelincourt, M.C.; Dhamelincourt, P.; Mazzah, A. Differential scanning calorimetric and Raman studies of a phase transition in $[\text{C}_3\text{H}_7\text{NH}_3]_2\text{SiF}_6$. *J. Raman Spectrosc.* **2004**, *35*, 261-265, <https://doi.org/10.1002/jrs.1145>.
2. Jeghnou, H.; Ouasri, A.; Rhandour, A.; Dhamelincourt, M.C.; Dhamelincourt, P.; Mazzah, A. Structural phase transition in $(n\text{-C}_4\text{H}_9\text{NH}_3)_2\text{SiF}_6$: DSC and Raman studies. *J. Raman Spectrosc.* **2003**, *34*, 126-130, <https://doi.org/10.1002/jrs.964>.
3. Ouasri, A.; Rhandour, A.; Dhamelincourt, M.C.; Dhamelincourt, P.; Mazzah, A.; Taibi, M. Infrared and Dielectric Studies of $[(\text{C}_2\text{H}_5)_4\text{N}]_2\text{SiF}_6$. *Phase Transitions* **2003**, *76*, 701-709, <https://doi.org/10.1080/0141159021000037240>.
4. Ouasri, A.; Rhandour, A.; Dhamelincourt, M.C.; Dhamelincourt, P.; Mazzah, A. Vibrational study of $(\text{CH}_3)_4\text{NSbCl}_6$ and $[(\text{CH}_3)_4\text{N}]_2\text{SiF}_6$. *Spectrochimica Acta Part A: Molecular and Biomolecular Spectroscopy* **2002**, *58*, 2779-2788, [https://doi.org/10.1016/S1386-1425\(02\)00019-7](https://doi.org/10.1016/S1386-1425(02)00019-7).
5. Ouasri, A.; Rhandour, A.; Dhamelincourt, M.C.; Dhamelincourt, P.; Mazzah, A.; Taibi, M. Structural phase transitions in $[(\text{C}_2\text{H}_5)_4\text{N}]_2\text{SiF}_6$: differential scanning calorimetry and Raman studies. *J. Raman Spectrosc.* **2002**, *33*, 715-719, <https://doi.org/10.1002/jrs.902>.
6. Reiß, G.J. Bis(diisopropylammonium) Hexafluorosilicate(IV). *Acta Crystallographica Section C* **1998**, *54*, 1489-1491, <https://doi.org/10.1107/S010827019800609X>.
7. Kosturek, B.; Czapla, Z.; Wb. Structure and Phase Transition of $[(\text{CH}_2\text{OH})_3\text{CNH}_3]_2\text{SiF}_6$. *Z. Naturforsch* **2003**, *58a*, 121-125.
8. Podsiadła, D.; Czupiński, O.; Rospenk, M.; Kosturek, B. Vibrational spectroscopic, optical and thermal properties of a deuterated ferroic crystal, $[(\text{CH}_2\text{OD})_3\text{CND}_3]_2\text{SiF}_6$ - An experimental and theoretical study. *Vib. Spectrosc* **2012**, *59*, 47-58, <https://doi.org/10.1016/j.vibspec.2011.12.015>.
9. Bozkurt, E.; Kartal, İ.; Karabulut, B. γ -irradiated $[(\text{CH}_3)_4\text{N}]_2\text{SiF}_6$ single crystal investigation by electron paramagnetic resonance technique. *J. Mol. Struct.* **2007**, *834-836*, 308-310, <https://doi.org/10.1016/j.molstruc.2006.09.034>.
10. Gudymenko, O.; Glushakov, V.; Boiko, O. Tetraalkylammonium Fluorosilicates as Precursors for Electrochemical Deposition of Silicon Coatings. Synthesis and Thermal Stability. *J. Chem. Chem. Eng.* **2015**, *9*, <https://doi.org/10.17265/1934-7375/2015.06.001>.
11. Ouasri, A.; Rhandour, A.; Dhamelincourt, M.-C.; Dhamelincourt, P.; Mazzah, A. The infrared and Raman spectra of ethylammonium hexafluorosilicate $[\text{C}_2\text{H}_5\text{NH}_3]_2\text{SiF}_6$. *Spectrochimica Acta Part A: Molecular and Biomolecular Spectroscopy* **2003**, *59*, 357-362, [https://doi.org/10.1016/S1386-1425\(02\)00165-8](https://doi.org/10.1016/S1386-1425(02)00165-8).
12. Ouasri, A.; Rhandour, A.; Dhamelincourt, M.-C.; Dhamelincourt, P.; Mazzah, A. Structure and vibrational study of the trimethylammonium hexafluorosilicate $[(\text{CH}_3)_3\text{NH}]_2\text{SiF}_6$ compound. *Spectrochimica Acta Part A: Molecular and Biomolecular Spectroscopy* **2003**, *59*, 851-857, [doi:https://doi.org/10.1016/S1386-1425\(02\)00231-7](https://doi.org/10.1016/S1386-1425(02)00231-7).
13. Gelmboldt, V.O.; Kravtsov, V.C.; Fonari, M.S. Ammonium hexafluoridosilicates: Synthesis, structures, properties, applications. *J. Fluorine Chem.* **2019**, *221*, 91-102, <https://doi.org/10.1016/j.jfluchem.2019.04.005>.
14. Anisimov, V.Y.; Shishkin, I.O.; Kravtsov, V.K. Synthesis, Structure, and Anticaries Activity of 2-Amino-4, 6-Dihydroxypyrimidinium Hexafluorosilicate. *Pharm. Chem. J.* **2018**, *52*, 606-610.
15. Gelmboldt, V.O.; Anisimov, V.Y.; Shyshkin, I.O.; Fonari, M.S.; Kravtsov, V.C. Synthesis, crystal structures, properties and caries prevention efficiency of 2-, 3-, 4-carboxymethylpyridinium hexafluorosilicates. *J. Fluorine Chem.* **2018**, *205*, 15-21, <https://doi.org/10.1016/j.jfluchem.2017.11.004>.
16. Gelmboldt, V.O.; Shyshkin, I.O.; Fonari, M.S.; Kravtsov, V.K. Synthesis, Crysta Structure, and Some Propertie of 4-Hydroxymethylpyridinium Hexafluorosilicate. *J. Struct. Chem.* **2019**, *60*, 1150-1155, <https://doi.org/10.1134/S0022476619070175>.
17. Gelmboldt, V.O.; Shyshkin, I.O.; Anisimov, V.Y.; Fonari, M.S.; Kravtsov, V.C. Bis(3-hydroxymethylpyridinium) hexafluorosilicate monohydrate as a new potential anticaries agent: Synthesis, crystal structure and pharmacological properties. *J. Fluorine Chem.* **2020**, *235*, 109547, <https://doi.org/10.1016/j.jfluchem.2020.109547>.

18. Anisimov, V.Y.; Shyshkin, I.O.; Levitsky, A.P.; Gelmboldt, V.O. Cariesprophylactic and periodontoprotective action of octenidine hexafluorosilicate in rats obtained with cariesogenic ration. *Farm. Zh.* **2019**, 86-95, <https://doi.org/10.32352/0367-3057.3.19.10>.
19. Gelmboldt, V.; Ognichenko, L.; Shyshkin, I.; Kuz'min, V. QSPR models for water solubility of ammonium hexafluorosilicates: analysis of the effects of hydrogen bonds. *Struct. Chem.* **2021**, 32, 309-319, <https://doi.org/10.1007/s11224-020-01652-3>.
20. Gelmboldt, V.O.; Lytvynchuk, I.V.; Shyshkin, I.O.; Ognichenko, L.N.; Kuz'min, V.E. Prognosis of biological activity and lipophilicity of some pyridine derivatives as components of anticaries agents. *Farm. Zh.* **2020**, 79-85, <https://doi.org/10.32352/0367-3057.2.20.08>.
21. Pristupa, B.V.; Shyshkin, I.O.; Rozhkovsky, Y.V.; Gelmboldt, V.O. Antiinflammatory activity of 2-, 3-, 4-carboxymethylpyridinium hexafluorosilicates on carrageenan model of inflammation. *Farm. Zh.* **2019**, 82-87, <https://doi.org/10.32352/0367-3057.4.19.09>.
22. Gelmboldt, V.O.; Anisimov, V.Y. Ammonium hexafluorosilicates: a new type of anticaries agents. *Farm. Zh.* **2018**, 48-69, <https://doi.org/10.32352/0367-3057.5-6.18.04>.
23. Elyoubi, M.; Ouasri, A.; Jeghnou, H.; Rhandour, A.; Dhamelincourt, M.C.; Dhamelincourt, P.; Mazzah, A. Vibrational spectroscopic study of alkylenediammonium hexachlorostannate compounds, $\text{NH}_3(\text{CH}_2)_n\text{NH}_3\text{SnCl}_6$ ($n = 3$ and 4). *J. Raman Spectrosc.* **2004**, 35, 1056-1062, <https://doi.org/10.1002/jrs.1254>.
24. Ouasri, A.; Elyoubi, M.S.D.; Guedira, T.; Rhandour, A.; Mhiri, T.; Daoud, A. Synthesis, DTA, IR and raman spectra of pentylenediammonium hexachlorostannate $\text{NH}_3(\text{CH}_2)_5\text{NH}_3\text{SnCl}_6$. *Spectrochimica Acta Part A: Molecular and Biomolecular Spectroscopy* **2001**, 57, 2593-2598, [https://doi.org/10.1016/S1386-1425\(01\)00431-0](https://doi.org/10.1016/S1386-1425(01)00431-0).
25. Elaoud, Z.; Chaabouni, S.; Daoud, A.; Kamoun, S. Chemical preparation and crystalline structure of ethylenediammonium hexafluorosilicate $\text{NH}_3(\text{CH}_2)_2\text{NH}_3\text{SiF}_6$. *C. r. acad. sci., Sér. II Méc. phys. chim. astron* **1995**, 320, 551-555.
26. Ouasri, A.; Rhandour, A.; Saadi, M.; El-Ammari, L. Crystal Structure of butylenediammonium hexafluorosilicate $\text{NH}_3(\text{CH}_2)_4\text{NH}_3\text{SiF}_6$. *Acta Cryst.* **2014**, E70, o174, doi:10.1107/S1600536814001068
27. Ouasri, A.; Rhandour, A.; Saadi, M.; El Ammari, L. Hexane-1, 6-diammonium hexafluorosilicate. *Acta Crystallogr. Sect. E: Struct. Rep. Online* **2014**, 70, o92-o93, <https://doi.org/10.1107/s1600536813034144>.
28. Ouasri, A.; Lambarki, F.; Rhandour, A.; Zahariev, T.K.; Trendafilova, N.; Georgieva, I. Solid state DFT modeling and vibrational characterisation of butylenediammonium and hexylenediammonium hexafluorosilicate, $\text{NH}_3(\text{CH}_2)_n\text{NH}_3\text{SiF}_6$ ($n=4$ and 6). *Vib. Spectrosc* **2017**, 88, 83-93, <https://doi.org/10.1016/j.vibspec.2016.11.006>.
29. Benzekri, Z.; Serrar, H.; Sibous, S.; Boukhris, S.; Ouasri, A.; Rhandour, A.; Souizi, A. Hybrid crystal $\text{NH}_3(\text{CH}_2)_4\text{NH}_3\text{SiF}_6$ as an efficient catalyst for the synthesis of benzoxazoles, benzimidazoles and benzothiazoles under solvent-free conditions. *Green Chemistry Letters and Reviews* **2016**, 9, 223-228, <https://doi.org/10.1080/17518253.2016.1242662>.
30. Benzekri, Z.; Serrar, H.; Said, B.; Ouasri, A.; Hassikou, A.; Rhandour, A.; Souizi, A. $\text{NH}_3(\text{CH}_2)_6\text{NH}_3\text{SiF}_6$ catalyzed highly efficient synthesis of benzimidazoles, benzoxazoles, benzothiazoles, quinoxalines and pyrimidin-2-ones/thiones. *French-Ukrainian Journal of Chemistry* **2017**, 5, 60-71, <https://doi.org/10.17721/fujcV5I1P60-71>.
31. Ouasri, A.; Elyoubi, M.S.D.; Rhandour, A.; Georgieva, I.; Zahariev, T.; Trendafilova, N.; Roussel, P. X-ray structures, solid state periodic DFT modeling and vibrational study of alkylenediammonium hexachlorostannates compounds $\text{NH}_3(\text{CH}_2)_n\text{NH}_3\text{SnCl}_6$ ($n = 3, 4, 5$). *J. Mol. Struct.* **2019**, 1177, 55-67, <https://doi.org/10.1016/j.molstruc.2018.09.040>.
32. El Adel, L.; Ouasri, A.; Rhandour, A.; Saadi, M.; El Ammari, L.; Hajji, L. Crystal structure, DSC, TGA and electrical studies of Bis (1,12-dodecamethylenediammonium hexachlorobismuthate chloride dihydrate $(\text{C}_{12}\text{H}_{30}\text{N}_2)_2\text{BiCl}_6 \cdot \text{Cl} \cdot 2\text{H}_2\text{O}$). *J. Mol. Struct.* **2020**, 1207, 127806, <https://doi.org/10.1016/j.molstruc.2020.127806>.
33. Jeghnou, H.; Ouasri, A.; Rhandour, A.; Dhamelincourt, M.C.; Dhamelincourt, P.; Mazzah, A.; Roussel, P. Structural phase transition in $[\text{NH}_3(\text{CH}_2)_5\text{NH}_3]\text{BiCl}_5$: thermal and vibrational studies. *J. Raman Spectrosc.* **2005**, 36, 1023-1028, <https://doi.org/10.1002/jrs.1400>.

34. Mousdis, G.A.; Papavassiliou, G.C.; Terzis, A.; Raptopoulou, C.P. Notizen: Preparation, Structures and Optical Properties of $[\text{H}_3\text{N}(\text{CH}_2)_6\text{NH}_3]\text{BiX}_5$ (X=I, Cl) and $[\text{H}_3\text{N}(\text{CH}_2)_6\text{NH}_3]\text{SbX}_5$ (X=I, Br). *Zeitschrift für Naturforschung B* **1998**, *53*, 927-932, <https://doi.org/10.1515/znb-1998-0825>.
29. Ouasri, A.; Rhandour, A.; Saadi, M.; El Ammari, L. catena-Poly [heptylenediammonium [[tetrachloridobismuthate (III)]- μ -chlorido]]. *Acta Crystallogr. Sect. E: Struct. Rep. Online* **2013**, *69*, m437, doi: 10.1107/S1600536813018102
35. Ouasri, A.; Jeghnou, H.; Rhandour, A.; Roussel, P. Structures and phases transition in hexylenediammonium pentachlorobismuthate (III) $[\text{NH}_3(\text{CH}_2)_6\text{NH}_3]\text{BiCl}_5$ crystal. *J. Solid State Chem.* **2013**, *200*, 22-29, <https://doi.org/10.1016/j.jssc.2013.01.002>.
36. Ouasri, A.; Jeghnou, H.; Rhandour, A.; Mazzah, A.; Roussel, P. X-ray, thermal and vibrational studies of two structural phases transition in hexylenediammonium pentachlorobismuthate (III) $[\text{NH}_3(\text{CH}_2)_6\text{NH}_3]\text{BiCl}_5$. *J. Mol. Struct.* **2012**, *1028*, 79-87, <https://doi.org/10.1016/j.molstruc.2012.05.061>.
37. Rhandour, A.; Ouasri, A.; Roussel, P.; Mazzah, A. Crystal structure and vibrational studies of butylenediammonium pentachlorobismuthate (III) hydrate $[\text{NH}_3(\text{CH}_2)_4\text{NH}_3]\text{BiCl}_5 \cdot \text{H}_2\text{O}$. *J. Mol. Struct.* **2011**, *990*, 95-101, <https://doi.org/10.1016/j.molstruc.2011.01.022>.
38. Ouasri, A.; Jeghnou, H.; Rhandour, A.; Dhamelincourt, M.-C ; Dhamelincourt, P. ; Mazzah, A. ; Roussel, P. Thermal and vibrational studies of propylenediammonium hexachlorobismuthate dihydrate $[\text{NH}_3(\text{CH}_2)_3\text{NH}_3]_3(\text{BiCl}_6)_2 \cdot 2\text{H}_2\text{O}$, *J. Raman spectroscopy*, **2005**, *36*, 791-796. <https://doi.org/10.1002/jrs.1365>
39. Benzekri, Z.; Sibous, S.; Serrar, H.; Ouasri, A.; Boukhris, S.; Ghailane, R.; Rhandour, A.; Souizi, A. $\text{NH}_3(\text{CH}_2)_5\text{NH}_3\text{BiCl}_5$ as a new hybrid and efficient catalyst for the synthesis of 1-(benzothiazolylamino)methyl-2-naphthol derivatives under solvent-free conditions. *J. Mol. Struct.* **2020**, *1202*, 127308, <https://doi.org/10.1016/j.molstruc.2019.127308>.
40. Benzekri, Z.; Sibous, S.; Serrar, H.; Ouasri, A.; Boukhris, S.; Rhandour, A.; Souizi, A. $\text{NH}_3(\text{CH}_2)_5\text{NH}_3\text{BiCl}_5$: an efficient and recyclable catalyst for the synthesis of benzoxazole, benzimidazole and benzothiazole heterocycles. *Journal of the Iranian Chemical Society* **2018**, *15*, 2781-2787, <https://doi.org/10.1007/s13738-018-1465-1>.
41. Gantar, D.; Rahten, A. Synthesis and characterization of $(\text{N}_2\text{H}_5)_2\text{SiF}_6$ and thermal analysis of $(\text{N}_2\text{H}_5)_2\text{SiF}_6$ and $\text{N}_2\text{H}_6\text{SiF}_6$. *Thermochim. Acta* **1986**, *108*, 149-155, [https://doi.org/10.1016/0040-6031\(86\)85086-9](https://doi.org/10.1016/0040-6031(86)85086-9).
42. Arianpour, F.; Arianpour, A.Ç.; Aali, B. Characterization and Properties of Sodium Hexa-Fluorosilicate and its Potential Application in the Production of Sodium Fluoride. *Silicon* **2020**, <https://doi.org/10.1007/s12633-020-00755-0>.
43. Healy, C.; Harvey-Reid, N.C.; Howard, B.I.; Kruger, P.E. Thermal decomposition of hybrid ultramicroporous materials (HUMs). *Dalton Transactions* **2020**, *49*, 17433-17439, <https://doi.org/10.1039/D0DT03852K>.
44. Anastassopoulou, J.D.; Berjot, M.; Marx, J.; Paleos, C.M.; Theophanides, T.; Alix, A.J.P. Raman spectra and conformational analysis of long-methylene-chain-diamine-copper complexes. *J. Mol. Struct.* **1997**, *415*, 225-237, [https://doi.org/10.1016/S0022-2860\(97\)00103-8](https://doi.org/10.1016/S0022-2860(97)00103-8).
45. Dhoub, I.; Ouasri, A.; Guionneau, P.; Pechev, S.; Elaoud, Z. Synthesis, molecular structure, vibrational studies, optical properties and electrical conduction mechanism of the new hybrid compound based on selenate. *Journal of Saudi Chemical Society* **2020**, *24*, 996-1009, <https://doi.org/10.1016/j.jscs.2020.10.007>.
46. Dhoub, I.; Ouasri, A.; Elaoud, Z. Disordered structures, vibrational spectroscopy, thermal behavior, and electrical properties of two new tetrachlorometallates complexes $[(\text{CH}_3\text{CH}_2\text{CH}_2)_4\text{N}]_2\text{MIIICl}_4$ with MII = Co and Mn. *Journal of Saudi Chemical Society* **2020**, *24*, 567-583, <https://doi.org/10.1016/j.jscs.2020.06.001>.